Appendices

Optimal noise reduction in 3D reconstructions of single particles using a volume-normalized filter

Charles V. Sindelar[1] and Nikolaus Grigorieff [2]

APPENDIX A: Adapting the SPW filter from 2D to 3D

Following the notation of Sindelar and Grigorieff (2011), we consider the case of image formation that conforms to the following model:

$$\rho_i^{2D}(x,y) = \mathrm{FT}^{-1}\{\mathrm{CTF}_i(h,k)\} * m(x,y) + n_i(x,y) \quad \text{(real space)} \qquad \text{(A1.1)}$$

$$F_i^{2D}(h,k) = \mathrm{FT}\{\rho_i^{2D}(x,y)\} = \mathrm{CTF}_i(h,k)M(h,k) + N_i(h,k) \qquad \text{(A1.1)}$$

(Fourier space)

where for the *i*'th image: $\rho_i^{2D}(x,y)$ is the observed projection density in the image, $m(x,y)$ is the projection of the noise-free 3D Coulomb potential of the particle, $\rho(\mathbf{r})$; $M(h,k)$ is the Fourier transform (FT) of $m(x,y)$, corresponding to a central section of $F(\mathbf{s}) = \mathrm{FT}\{\rho(\mathbf{r})\}$. We employ a commonly used noise model in which all noise effects are accounted for by a single term, $n_i(x,y)$ (this simplification is justified, as noted previously (Sindelar and Grigorieff, 2011), by the expected dominance of shot noise from the measurement process itself over other noise sources). $N_i(h,k)$ is the corresponding FT of $n_i(x,y)$. The contrast transform function term is here written as $\mathrm{CTF_i}(h,k)$.

Wiener filter for a 3D toy problem

By the projection theorem (Radon, 1917), the FT of each measured image samples a two-dimensional plane through the 3D FT of the molecular map (a "Fourier slice"), where the orientation of the slice is defined by the viewing orientation for the image (usually specified by Euler angles ψ, φ, θ). Thus, in principle, a sufficiently large data set of image FTs could be used to measure all values in the 3D FT, and inverse FT would complete the 3D reconstruction problem. In practice, the plane defined by a Fourier slice

almost never coincides with the discrete 3D FT (DFT) grid that is utilized in computational treatments, so that the discrete grid points themselves are not precisely sampled. We address this problem in the current work by using a "gridding" approach in which each measurement on the Fourier slice is averaged with its nearest neighbor on the discretely sampled 3D DFT grid, followed by a compensatory post-processing step (Appendix B).

For the moment, however, we choose to idealize the reconstruction problem by considering a "toy" data set for which each measurement falls exactly on the 3D DFT grid. A large set of randomly oriented Fourier slices will thus provide a variable number of noisy measurements, $F^{2D}_{i,hkl}$, with CTF values $\mathrm{CTF}_{i,hkl}$ (i=1, 2, … N_{hkl}) for each value $F^{3D}\left(\mathbf{s}_{hkl}\right)$ on the 3D Fourier grid (one way to approximate such a case with arbitrary accuracy would be to pad the 3D volume to be reconstructed by an arbitrarily large amount). Here, $\mathbf{s}_{hkl}$ represents a discrete grid point in the 3D DFT having integer indices *hkl*, and N_{hkl} is the number of measurements contributing to grid point $\mathbf{s}_{hkl}$ (corresponding to how many Fourier slices contribute to this grid point; this is related to the number of interpolated measurements n_{hkl} contributing to a grid point, see below). The values of $F^{2D}_{i,hkl}$ are related to $F^{2D}_{i}\left(h,k\right)$ (Eq. (A1.2) but are now assigned to grid point $\mathbf{s}_{hkl}$. Thus, this idealized scenario emulates the 3D reconstruction problem, but avoids any errors associated with fractional coordinates and "gridding" (see Appendix B). To reduce the error when forming a reconstructed map from this 'toy' data set, we write an expression for the expected squared error:

$$\text{Error} = \left\langle \left| \rho(\mathbf{r}) - \rho^{W}(\mathbf{r}) \right|^2 \right\rangle \text{ (where } \rho^{W} \text{ is the map estimate)} \qquad \text{(A1.3)}$$

and solve for a set of linear coefficients that will form an ideally weighted sum of the Fourier space data points, minimizing the average error. In the absence of additional information, the least squares estimate is (Saxton (1978), note that this result was presented by Saxton specifically for the case 2D images, but readily generalizes to 3D):

$$M(\mathbf{s}_{hkl}) \approx F^{\text{LSQ}}(\mathbf{s}_{hkl}) = \text{DFT}\left\{\rho^{\text{LSQ}}(\mathbf{r})\right\} = \frac{\sum_{i=1}^{N_{hkl}} \left\{\text{CTF}_{i,hkl}\right\}^{*} F_{i,hkl}^{\text{2D}}}{\varepsilon + \sum_{i=1}^{N_{hkl}} \left|\text{CTF}_{i,hkl}\right|^2} \qquad \text{(A1.4)}$$

Here, we have introduced a small constant term, ε that prevents division by zero. For the current work we have selected the value $\varepsilon = 0.1$, which in our numeric tests was large enough to prevent numeric errors but too small to generate any substantial filtering effect on the reconstructions, as judged by insensitivity of reconstruction statistics to perturbations of ε around the chosen value (results not shown). If estimates of the signal-to-noise ratio (SNR) of the data measurements are available, the result is a "Wiener filter" (Saxton, 1978), expressed as follows:

$$F^{W}(\mathbf{s}_{hkl}) = \text{DFT}\left\{\rho^{W}(\mathbf{r})\right\} = \frac{\sum_{i=1}^{N_{hkl}} \left\{\text{CTF}_{i,hkl}\right\}^{*} F_{i,hkl}^{\text{2D}}}{\sum_{i=1}^{N_{hkl}} \left|\text{CTF}_{i,hkl}\right|^2 + 1/\text{SSNR}(s_{hkl})} \qquad \text{(A1.5)}$$

(bold symbols are vectors and italicized non-bold symbols refer to the length of the corresponding vectors). Here SSNR refers to the spectral SNR of the measured data, $\text{SSNR}(s) \equiv \left\langle \left|M(\mathbf{s})\right|^2 \right\rangle_{\mathbf{s}_{hk} \in \text{S}^{2\text{D}}(s)} \Big/ \left\langle \left|N_i(\mathbf{s})^2\right| \right\rangle_{\mathbf{s}_{hk} \in \text{S}^{2\text{D}}(s)}$, and is expressed in terms of the average value of the SNR in resolution ring $\text{S}^{2\text{D}}$ with central radius *s* and containing 2D grid

points $\mathbf{s}_{hk} \in \mathrm{S}^{2\mathrm{D}}(s)$. We note that while the measured data come from 2D DFT's of the images, the data also represent measurements of central sections in the 3D DFT of the particle. The SSNR function can therefore be used for Wiener filtering in 2D (Saxton, 1978) as well as 3D (Eq. (A1.5)). Furthermore, it is important to realize that the SSNR refers to the measured data *before* averaging to obtain a reconstruction. The above expression for the Wiener filter differs from the form presented earlier for the case of 2D image averaging (Saxton, 1978) only by its extension to 3D coordinates, and by allowing the number of Fourier samples N_{hkl} to vary from voxel to voxel.

Single-particle Wiener filter for the 3D toy problem

As was previously observed for the 2D case (Sindelar and Grigorieff, 2011), the overall SNR of a 3D map of an isolated single particle depends on the bounding box dimension. The noise energy in the box increases proportional to the total box volume, while the signal energy (due to the particle) remains constant. Consequently, SSNR cannot be consistently defined and application of Eq. (A1.5) leads to progressively greater over-filtering of the resulting particle density as the bounding box size is increased. We emphasize that this over-filtering effect is a natural consequence of the error-minimizing property of Eq. (A1.5): as the box size grows, the noisy solvent region increasingly dominates the error sum, thus requiring a stronger filter in order to minimize the mean-squared error at all points in the volume (see Sindelar and Grigorieff (2011)).

As we did previously for the 2D case, we address the above problem with the Wiener

filter by reframing the problem to optimize the density of a single particle reconstruction: we now seek the filter that minimizes the error within the particle region only, utilizing a binary enveloping function $\mathrm{env}_{3D}(\mathbf{r})$ that excludes the solvent region:

$$\text{Error} = \left|\mathrm{env}_{3D}(\mathbf{r}) \cdot \left\{\rho(\mathbf{r}) - \rho^{\mathrm{SPW}}(\mathbf{r})\right\}\right|^2 = \left|\rho(\mathbf{r}) - \mathrm{env}_{3D}(\mathbf{r}) \cdot \rho^{\mathrm{SPW}}(\mathbf{r})\right|^2 \tag{A1.6}$$

Unlike $\rho^{\mathrm{W}}(\mathbf{r})$ in Eq (A1.5), $\rho^{\mathrm{SPW}}(\mathbf{r})$ represents the estimate that minimizes the error inside the envelope. We may now proceed identically as was done for the 2D case in order to obtain a modified filter expression, by assuming several conditions are approximately satisfied. Briefly, we assume that (1) a sufficiently large amount of data was collected such that the map estimate $\rho^{\mathrm{SPW}}(\mathbf{r})$ is approximately localized within the binary enveloping function; (2) the noise found in the data has relatively modest frequency dependence and (3) the particle radius is non-negligible relative to the box dimension. Repeating the derivation in Sindelar and Grigorieff (2011) but substituting 3D functions in place of 2D functions leads to the following approximate solution for the least squares linear filter expression:

$$F^{\mathrm{SPW}}(\mathbf{s}_{hkl}) = \mathrm{DFT}\left\{\rho^{\mathrm{SPW}}(\mathbf{r})\right\} = \frac{\sum_{i=1}^{N_{hkl}} \left\{\mathrm{CTF}_{i,hkl}\right\}^* F^{\mathrm{2D}}_{i,hkl}}{\sum_{i=1}^{N_{hkl}} \left|\mathrm{CTF}_{i,hkl}\right|^2 + 1/\mathrm{PSSNR}(s_{hkl})} \tag{A1.7}$$

$$\mathrm{PSSNR}(s) = \frac{1}{f_{\mathrm{particle}}} \mathrm{SSNR}(s) \tag{A1.8}$$

$$f_{\mathrm{particle}} = \left\langle \mathrm{env}^2_{3D}(\mathbf{r}) \right\rangle_{\mathbf{r} \in V} \tag{A1.9}$$

As with the 2D single-particle Wiener filter, this 3D version compensates for the presence of extra noise energy in the solvent region by scaling up the SNR term. The

principal difference between the 3D and 2D incarnations of the filter is that here f_{particle} is computed over a 3D envelope function, defining the relative proportion of solvent in the reconstructed box. As shown in Fig. A.1, we validated Eqs. (A1.7) – (A1.9) via numeric tests of synthetic noisy 3D data sets (embodying the "3D toy problem", above), and confirmed that the reconstruction error was minimized with respect to f_{particle}, as we demonstrated previously for the analogous 2D case (Sindelar and Grigorieff, 2011).

A

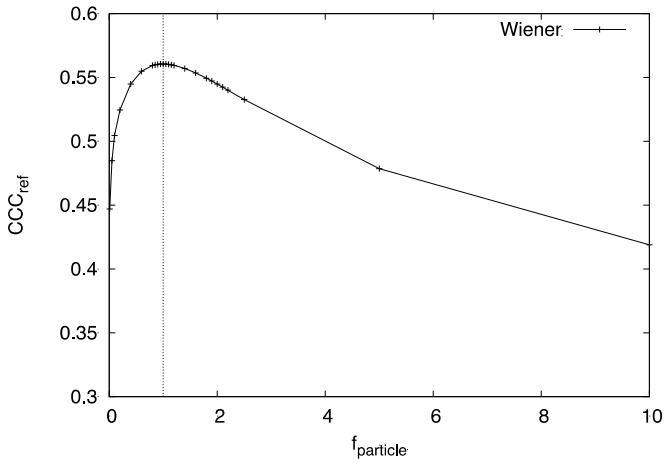

B

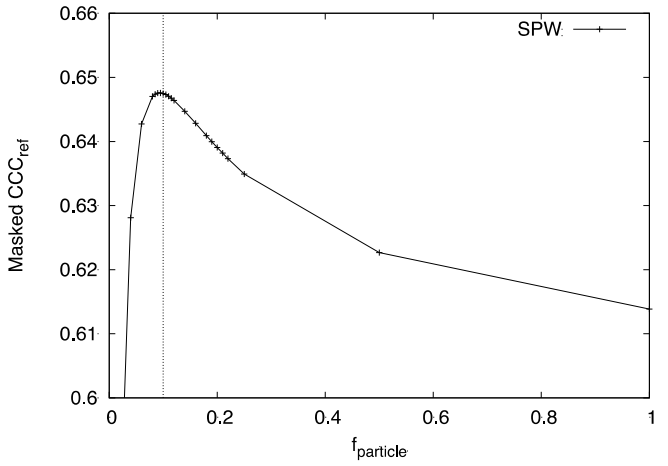

Figure A.1 Validation of the SPW filter using a 3D 'toy' data set. Values of $F^{2D}_{i,hkl}$ were generated by adding randomly generated white noise to structure factors taken from the 3D FFT of the same noise-free synthetic volume used in other computations here (see Methods). No CTF modulation was considered ($CTF_{i,hkl}$ were all equal to 1). The number of measurements per Fourier voxel, N_{hkl}, was made identical (for each *hkl*) to the number of interpolated measurements n_{hkl} found in our gridded reconstructions made from noisy 2D projection images.

A. Unmasked cross correlation coefficients between the noise-free reference volume and

a series of reconstructions generated using Eq. (A1.7), with varying values of f_{particle}. The correlation is maximized at $f_{\text{particle}} = 1$, which corresponds to the original Wiener filter, Eq. (A1.5). Thus, these calculations show that the Wiener filter yields the minimum overall error (including the solvent region), with respect to scaling of its SSNR term.

B. Masked cross correlation coefficients between the noise-free reference volume and the same series of reconstructions as in panel A (mask from Fig. 2E was used). The correlation is maximized at $f_{\text{particle}} = 0.10$, which is identical to the value of f_{mask} we compute for the chosen mask. Thus, the SPW filter minimizes error within the defined mask region, for the given mask size.

APPENDIX B: Extending the SPW theory for gridded 3D reconstruction

The *i*'th image in a cryo-EM data set, following DFT and rotational transformation according to the known or estimated Euler angles (φ, θ, ψ) (describing the projection direction), consists of a list of discrete measurements that lie on a plane in 3D Fourier space:

$$F_i^{2D}(h,k) = \mathrm{CTF}_i(h,k)M(h,k) + N_i(h,k) \qquad \text{(A2.1)}$$

Due to the arbitrary orientation of this plane, the coordinates $\mathbf{s}_{i,hk}$ of the measurements rarely coincide with the 3D grid points $\mathbf{s}_{hkl}$. Thus, a series of such images will yield an irregular cloud of point measurements spread throughout 3D Fourier space (up to the Nyquist sampling limit of the images).

In order to apply the 3D inverse DFT, this measurement cloud must be extrapolated onto the 3D cubic grid of DFT coordinates. The gridding method (Penczek, 2010) accomplishes this extrapolation by convolving the cloud of measurements with a "kernel" function (for example, a Gaussian function with a half-width of a few Fourier pixel dimensions), followed by sampling of the resulting blurred function on the DFT grid. This combined operation effectively gathers all measurements within a specified radius onto a given DFT grid point, as a weighted average. A subsequent inverse DFT operation yields a real-space map whose values are, due to the preceding convolution operation, effectively multiplied by the inverse DFT of the kernel function (which we will refer to as the point-spread function or PSF). Thus, to undo the effects of the convolution/sampling step, the final step of gridding is a division of the real-space map by the PSF, yielding an approximation of the desired molecular map.

Here we implement a very simple form of gridding in which the kernel function is a 3D rectangle function Rect (namely a cube having a linear dimension equal to the Fourier grid spacing). Thus, the initial (convolution) step in the gridding process estimates the quantity

$$F^{\text{grid}}(\mathbf{s}_{hkl}) = \delta(\mathbf{s}_{hkl}) \cdot [\text{Rect}(\mathbf{s}) * F(\mathbf{s})] \,. \qquad \text{(A2.2)}$$

Here, $\delta(\mathbf{s}_{hkl})$ is the 3D Dirac delta function. In order to account for non-uniform measurement density in Fourier space, we normalize the convolution sums at each voxel by dividing by the number of measurements n_{hkl} that contribute to these respective locations. In the case of ideal images (in the absence of noise and having an ideal CTF equal to unity for all **s**), the first step of our gridding implementation would therefore be a straight average of nearest neighbor measurements for each grid point $\mathbf{s}_{hkl}$

$$F^{\text{grid}}(\mathbf{s}_{hkl}) = \delta(\mathbf{s}_{hkl}) \cdot [\text{Rect}(\mathbf{s}) * F(\mathbf{s})] \approx \frac{\sum_{i=1}^{n_{hkl}} \tilde{F}^{2\text{D}}_{i,hkl}}{n_{hkl}} \qquad \text{(A2.3)}$$

with

$$\sum_{i=1}^{n_{hkl}} \tilde{F}^{2\text{D}}_{i,hkl} = \sum_{j=1}^{N_{\text{images}}} \sum_{h',k'} \text{Rect}(\mathbf{s}_{j,h'k'} - \mathbf{s}_{hkl})^{*} \tilde{F}^{2\text{D}}_{j}(h',k'). \qquad \text{(A2.4)}$$

The tilde in $\tilde{F}^{2\text{D}}_{j}$ symbolizes the Fourier terms of a noise-free idealized image that is not affected by CTF modulation to distinguish it from the Fourier terms $F^{2\text{D}}_{j}$ of a noisy experimental image (see below). We will use the abbreviated notation defined by Eq. (A2.4) in the following and throughout the main manuscript, for all sums that result from the convolution with the rectangle function Rect.

We note that the approximation in Eq. (A2.3) results from a general difficulty encountered in gridding algorithms to account for irregular sampling of the FT. While values of the FT F of the noise-free volume are evenly distributed between the discrete 3D grid points $\mathbf{s}_{hkl}$, the results of the convolution described by Eq. (A2.4) must be weighted to account for the irregular sampling. The simple weighting by $1/n_{hkl}$ (Eq. (A2.3)) will tend to skew the estimate $F^{\text{grid}}(\mathbf{s}_{hkl})$ towards values of F found in the most densely measured regions near a given $\mathbf{s}_{hkl}$. To compensate for this effect, additional weighting terms (proportional to the local measurement density) can be introduced within the sum in Eq. (A2.3) in order to yield a more accurate estimate of the convolution in Eq. (A2.2) (Penczek et al., 2004). However, such "gridding weights" are not necessarily beneficial in the presence of large amounts of noise, particularly when F varies slowly through the extent of the kernel function; moreover, schemes to estimate the local measurement density add substantial algorithmic complexity. We therefore opted not to implement gridding weights in our scheme, and instead padded images and volumes by a factor of two in order to reduce the variability of F on the scale of the kernel function size (equal to the grid spacing, for the rectangle kernel function used here).

Application of Eq. (A2.3) by itself for 3D reconstruction is commonly referred to in the literature as nearest neighbor interpolation (Penczek, 2010). However, having connected Eq. (A2.3) to the convolution product in Eq. (A2.2), we may now proceed to the second stage of gridding. Following inverse DFT of F^{grid}, the effects of the kernel convolution may be reversed by dividing the resulting map by the PSF, in this case equal to a sinc function (the inverse DFT of the rectangle function):

$$\rho^{\text{grid}}(\mathbf{r}) = \frac{\text{DFT}^{-1}\left[F^{\text{grid}}(\mathbf{s})\right]}{\text{DFT}^{-1}\left(\text{Rect}(\mathbf{s})\right)} = \frac{\text{DFT}^{-1}\left[F^{\text{grid}}(\mathbf{s})\right]}{\text{sinc}(\pi x / L)\text{sinc}(\pi y / L)\text{sinc}(\pi z / L)} \qquad \text{(A2.5)}$$

where L is the linear dimension of the volume and x,y,z are the components of $\mathbf{r}$.

We now modify our expression for F^{grid} to account for the presence of CTF modulation and noise by adapting Eq. (A1.4) to form the least squares estimate for the series of measurements tallied in Eq. (A2.3):

$$F^{\text{LSQ}}(\mathbf{s}_{hkl}) = \delta(\mathbf{s}_{hkl}) \cdot \left[\text{Rect}(\mathbf{s}) * F(\mathbf{s})\right] \approx \frac{\sum_{i=1}^{n_{hkl}} \left\{\text{CTF}_{i,hkl}\right\}^* F_{i,hkl}^{\text{2D}}}{\varepsilon + \sum_{i=1}^{n_{hkl}} \left|\text{CTF}_{i,hkl}\right|^2}. \qquad \text{(A2.6)}$$

As before (Eq. (A1.4)), we have introduced a small constant term, ε.

Following the example of Eq. (A1.5), we may also adapt Eq. (A2.6) to form a filtered estimate of the first gridded reconstruction step:

$$F^{\text{W}}(\mathbf{s}_{hkl}) \approx \frac{\sum_{i=1}^{n_{hkl}} \left\{\text{CTF}_{i,hkl}\right\}^* F_{i,hkl}^{\text{2D}}}{\sum_{i=1}^{n_{hkl}} \left|\text{CTF}_{i,hkl}\right|^2 + 1/\text{SSNR}(s_{hkl})} \qquad \text{(A2.7)}$$

(a similar expression can be written for F^{SPW}). The above expression yields the linear transformation of the data having the least squares expected error. However, the error is not minimized against $F(\mathbf{s})$ itself but rather for $\text{Rect}(\mathbf{s}) * F(\mathbf{s})$. Thus, after applying the final gridding correction (division by the sinc function, Eq. (A2.5)) the error in the final gridded reconstruction is no longer strictly minimized; instead, the gridding correction boosts noise levels near the volume boundaries (results not shown). In order to mitigate this issue, we padded

all images and volumes by a factor of two, so that the sinc correction factor remained close to one in the vicinity of the particle (the maximum value of this correction is at the original volume boundary, which becomes +/- L/4 after 2-fold padding, so that the correction factor would be $\mathrm{sinc}\left(\frac{\pi L/4}{L}\right)^{-1} = \left(\frac{\sin(\pi/4)}{\pi/4}\right)^{-1} = 1.11$).

APPENDIX C: Estimating the image SSNR from masked FSC calculations

Following the approach given by Sindelar and Grigorieff (2011) for aligned 2D images, we begin by expressing the expectation value of $\mathrm{FSC}_{\mathrm{mask}}(s)$ in terms of the signal and noise components from two noisy half data set reconstructions, each multiplied in real space by the soft-edged masking function $\mathrm{env}_{\mathrm{mask}}(\mathbf{r})$:

$$\left\langle \mathrm{FSC}_{\mathrm{mask}}(s) \right\rangle \approx \frac{\left\langle \sum_{\mathbf{s}_{hkl} \in \mathrm{S}(s)} \left[\mathrm{ENV}_{\mathrm{mask}}(\mathbf{s}_{hkl}) * \left(F(\mathbf{s}_{hkl}) + N_1(\mathbf{s}_{hkl}) \right) \cdot \mathrm{ENV}_{\mathrm{mask}}(\mathbf{s}_{hkl}) * \left(F(\mathbf{s}_{hkl}) + N_2(\mathbf{s}_{hkl}) \right) \right] \right\rangle}{\sqrt{\left\langle \sum_{\mathbf{s}_{hkl} \in \mathrm{S}(s)} \mathrm{ENV}_{\mathrm{mask}}(\mathbf{s}_{hkl}) * \left(F(\mathbf{s}_{hkl}) + N_1(\mathbf{s}_{hkl}) \right) \right\rangle^2 \left\langle \sum_{\mathbf{s}_{hkl} \in \mathrm{S}(s)} \mathrm{ENV}_{\mathrm{mask}}(\mathbf{s}_{hkl}) * \left(F(\mathbf{s}_{hkl}) + N_2(\mathbf{s}_{hkl}) \right) \right\rangle^2}} \qquad \text{(A3.1)}$$

where S denotes a one Fourier voxel thick shell with central radius *s*; N_1 and N_2 are noise components with the same variance, corresponding to Fourier terms of the first and second reconstruction (respectively); and $\mathrm{ENV}_{\mathrm{mask}}$ is the FT of $\mathrm{env}_{\mathrm{mask}}$. If we assume that N_1 and N_2 are uncorrelated, which can be achieved by performing independent 3D structure refinement on the two half data sets, then Eq. (A3.1) reduces to

$$\left\langle \mathrm{FSC}_{\mathrm{mask}}(s) \right\rangle = \frac{\left\langle \sum_{\mathbf{s}_{hkl} \in \mathrm{S}(s)} F(\mathbf{s}_{hkl})^2 \right\rangle}{\left\langle \sum_{\mathbf{s}_{hkl} \in \mathrm{S}(s)} F(\mathbf{s}_{hkl})^2 \right\rangle + \left\langle \sum_{\mathbf{s}_{hkl} \in \mathrm{S}(s)} \mathrm{ENV}_{\mathrm{mask}}(\mathbf{s}_{hkl})^2 * N(\mathbf{s}_{hkl})^2 \right\rangle} \qquad \text{(A3.2)}$$

where we have used the following: (1) the noise-free map $\rho(\mathbf{r})$ is unchanged by the mask multiplication, hence $\mathrm{ENV}_{\mathrm{mask}}(s) * F(s) = F(s)$, (2) the noise terms are uncorrelated with the signal terms; and (3) the noise is now represented by a *N*, which stands for an arbitrary realization of the noise in a half data set reconstruction. If we now assume that the noise term varies slowly in *s* compared with the $\mathrm{ENV}_{\mathrm{mask}}(s)$ term, as is expected for single-particle cryo-EM data sets (Sindelar and Grigorieff, 2011), then the right-hand term in the denominator of Eq. (A3.2) can be approximated as:

$$\left\langle \sum_{\mathbf{s}_{hkl} \in \mathrm{S}(s)} \mathrm{ENV}_{\mathrm{mask}}(\mathbf{s}_{hkl})^2 * N_1(\mathbf{s}_{hkl})^2 \right\rangle \approx f_{\mathrm{mask}} \left\langle \sum_{\mathbf{s}_{hkl} \in \mathrm{S}(s)} N(\mathbf{s}_{hkl})^2 \right\rangle \qquad \text{(A3.3)}$$

where $f_{\mathrm{mask}} = \left\langle \mathrm{env}^2_{\mathrm{mask}}(\mathbf{r}) \right\rangle_{\mathbf{r} \in V}$. Thus, we can write:

$$\left\langle \mathrm{FSC}_{\mathrm{mask}}(s) \right\rangle \approx \frac{\left\langle \sum_{\mathbf{s}_{hkl} \in \mathrm{S}(s)} F(\mathbf{s}_{hkl})^2 \right\rangle}{\left\langle \sum_{\mathbf{s}_{hkl} \in \mathrm{S}(s)} F(\mathbf{s}_{hkl})^2 \right\rangle + f_{\mathrm{mask}} \left\langle \sum_{\mathbf{s}_{hkl} \in \mathrm{S}(s)} N(\mathbf{s}_{hkl})^2 \right\rangle} \qquad \text{(A3.4)}$$

Rewriting the above expression in terms of the SSNR of the reconstruction,

$\mathrm{SSNR}_{\mathrm{final}}(s) = 2\left\langle \sum_{\mathbf{s}_{hkl} \in \mathrm{S}(s)} F(\mathbf{s}_{hkl})^2 \right\rangle \Big/ \left\langle \sum_{\mathbf{s}_{hkl} \in \mathrm{S}(s)} N(\mathbf{s}_{hkl})^2 \right\rangle$ (where we note that the SSNR is doubled by combining the two half data sets) we now arrive at the following expression:

$$\left\langle \mathrm{FSC}_{\mathrm{mask}}(s) \right\rangle \approx \frac{\mathrm{SSNR}_{\mathrm{final}}(s) \big/ f_{\mathrm{mask}}}{\mathrm{SSNR}_{\mathrm{final}}(s) \big/ f_{\mathrm{mask}} + 2} \tag{A3.5}$$

We rewrite the above result to express the SSNR in terms of the masked FSC:

$$\mathrm{SSNR}_{\mathrm{final}}(s) \approx f_{\mathrm{mask}} \frac{2\left\langle \mathrm{FSC}_{\mathrm{mask}}(s) \right\rangle}{1 - \left\langle \mathrm{FSC}_{\mathrm{mask}}(s) \right\rangle} \tag{A3.6}$$

which is the 3D analog of the result for 2D images (Sindelar and Grigorieff, 2011).

To relate $\mathrm{SSNR}_{\mathrm{final}}$ to the SSNR of the images, we refer to Eq. (A2.6), which expresses the gridded FT F^{LSQ} as a weighted sum over Fourier space measurements from individual images. Similar to the case of aligned 2D images (see Sindelar and Grigorieff (2011)), the noise variance in F^{LSQ} reduces proportional to the sum of squared CTF terms. Thus, to recover an estimate of the data SNR we can write

$$\mathrm{SSNR}(s) \approx f_{\mathrm{mask}} \frac{\sum_{\mathbf{s}_{hkl} \in S(s)} 1}{\sum_{\mathbf{s}_{hkl} \in \mathrm{S}(s)} \sum_{i=1}^{n_{hkl}} \left| \mathrm{CTF}_{i,hkl} \right|^2} \cdot \frac{2\mathrm{FSC}_{\mathrm{mask}}(s)}{(1 - \mathrm{FSC}_{\mathrm{mask}}(s))} \tag{A3.7}$$

Here it is worth repeating the observation made in Appendix A that the 2D image DFT's are equivalent to central sections of the 3D DFT, so that the SSNR in either case is also equivalent. We note that this last step involves an additional approximation, related to the fact that the summed Fourier terms in Eq. (A2.6) are an estimate of the continuously varying FT F convolved over a rectangle kernel function. Consequently, the noise-free signal component in F^{LSQ} is attenuated somewhat and so the SSNR from Eqs. (A3.6) – (A3.7) will be underestimated. The two-fold padding we employed in our reconstruction algorithm, however, reduces this variability over the extent of the kernel function, increasing the accuracy of the SSNR estimate.

References

Penczek, P.A. (2010). Fundamentals of three-dimensional reconstruction from projections. Meth. Enzymol *482*, 1–33.

Penczek, P.A., Renka, R., and Schomberg, H. (2004). Gridding-based direct Fourier inversion of the three-dimensional ray transform. J Opt Soc Am A Opt Image Sci Vis *21*, 499–509.

Radon, J. (1917). Über die Bestimmung von Funktionen durch ihre Integralwerte längs gewisser Manningfaltigkeiten. Math. Phys. Klasse *69*, 262–277.

Saxton, W.O. (1978). Computer techniques for image processing in electron microscopy (Academic Press (New York)).

Sindelar, C.V., and Grigorieff, N. (2011). An adaptation of the Wiener filter suitable for analyzing images of isolated single particles. J. Struct. Biol. *176*, 60–74.